Mixed valence of a delocalized system: A resonance Raman study of the tetracyanoquinodimethane radical anion

ARTICLE *in* JOURNAL OF PHYSICAL ORGANIC CHEMISTRY · MAY 2009

Impact Factor: 1.38 · DOI: 10.1002/poc.1518

Research Article

Journal of Physical Organic Chemistry

Received: 1 October 2008, Revised: 26 November 2008, Accepted: 2 December 2008, Published online in Wiley InterScience: 20 February 2009

(www.interscience.wiley.com) DOI 10.1002/poc.1518

Mixed valence of a delocalized system: a resonance Raman study of the tetracyanoquinodimethane radical anion

Ryan M. Hoekstra[a], Jeffrey I. Zink[a], João P. Telo[b] and Stephen F. Nelsen[c]*

The optical absorption spectrum and resonance Raman enhancement of the lowest energy absorption band of K^+7,7,8,8-tetracyanoquinodimethane$^-$ (TCNQ) are reported and examined in the mixed valence (MV) framework. The absorption spectrum is assigned, in accordance with previous work, using Koopmans-based calculations and the neighboring orbital model is constructed from the adiabatic orbital energies. Calculated fits of the lowest energy absorption band and the corresponding resonance Raman enhancement profiles are made using the time-dependent theory of spectroscopy. Copyright © 2009 John Wiley & Sons, Ltd.

Supporting information may be found in the online version of this article.

Keywords: TCNQ; mixed valence; resonance Raman; tetracyanoquinodimethane; reorganization energy

INTRODUCTION

Ground state mixed valence (MV) is a familiar concept that was developed by inorganic chemists in the 1960s.[1–3] In the simplest case, two charge-bearing units (**M**) consisting of a metal center are connected by a bridging divalent ligand (**B**) and the oxidation level is odd, so that the charges on the **M** groups might be different. When the charges are different, it is called a Robin–Day Class II system,[1] and may usefully be considered to be represented as $\mathbf{M}^n$–**B**–$\mathbf{M}^{n\pm1}$. They are the most revealing electron transfer (ET) systems known because of Hush's remarkably simple method for extracting both the reorganization energy, λ (which is the energy of the charge-transfer band maximum, $\overline{\nu}_{max}$), and the electronic coupling, V_{ab}, in the two-state model that Marcus introduced for ET reactions,[4,5] which allows calculating the barrier for ET and hence the rate constant.[5] Metal-centered examples have such low barriers that the rate constants for ET within MV compounds for which the charge transfer band is intense enough to measure accurately have not been determined. Nelsen and coworkers used the large reorganization energies of dinitrogen organic charge-bearing units to measure rate constants for all-organic examples of Class II MV compounds using electron spin resonance, demonstrating that Hush's method for extracting V_{ab} is as accurate since the electron-transfer distance can be estimated.[6,7] When V_{ab} exceeds $\lambda/2$, the barrier to ET disappears, the system becomes charge-delocalized, and is called a Robin–Day Class III system. If the two-state model is applied unaltered to the low energy band observed for a Class III compound, $\overline{\nu}_{max} \sim 2V_{ab}$, as first pointed out by Creutz,[8] and has been extensively applied by many workers to the lowest energy intense absorption band for Class III MV systems,[9–12] and is also employed in the Generalized Mulliken–Hush theory of Cave and Newton.[13,14] As has been well known for many years, the transition that people have called an MV one for Class III compounds is between molecular orbitals (MOs) of different symmetry. This means that they cannot be related to each other by a single electronic coupling; orbitals of different symmetry do not split each other. The simplest model that could possibly give realistic transitions involves four states and two electronic couplings, which we described as the neighboring orbital model.[21,15,16] The ground state of Class III compounds has a single minimum, and equal charges on the charge-bearing units, but the diabatic surfaces for the excited state could be represented by a Marcus–Hush diagram (Fig. 1) because either charge-bearing unit could donate charge to (as in diarylhydrazine radical cations)[17–20] or accept charge from the bridge (as in dinitroaromatic radical anions[21] and the radical anion case we discuss here).

This work concerns 7,7,8,8-tetracyanoquinodimethane (TCNQ) first published by workers from DuPont in 1962.[22] The radical anion salts of this electron-accepting molecule show a wide range of interesting electronic and magnetic properties. Metal $\mathbf{1}^{\bullet-}$ salts display electric conductivity in a wide range of temperatures[23,24] and the $\mathbf{TTF}^{\bullet+}$—$\mathbf{1}^{\bullet-}$ charge-transfer salt

* *Correspondence to: S. F. Nelsen, Department of Chemistry, University of Wisconsin, 1101 University Avenue, Madison, WI 53706-1396, USA. E-mail: nelsen@chem.wisc.edu*

a *R. M. Hoekstra, J. I. Zink*
Department of Chemistry and Biochemistry, University of California Los Angeles, California 90095, USA

b *J. P. Telo*
Centro de Química Estrutural, Instituto Superior Técnico, Av. Rovisco Pais, 1049-001 Lisboa, Portugal

c *S. F. Nelsen*
Department of Chemistry, University of Wisconsin, 1101 University Avenue, Madison, Wisconsin 53706-1396, USA

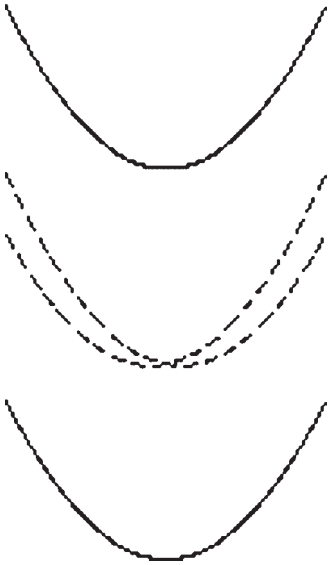

Figure 1. Cartoon representation of a Class III MV compound which has a large enough effective electronic coupling between the diabatic surfaces (dashed lines) to produce single minimum surfaces for the split excited state adiabats (shown as solid lines)

(where TTF stands for tetrathiafulvalene) was the first fully organic 'metal' conductor reported, showing metallic behavior down to 54 K.[25] The decamethyl-ferrocenium-$\mathbf{1}^{\bullet-}$ charge-transfer salt orders as a metamagnet below 2.55 K,[26,27] and the magnetic properties of numerous other $\mathbf{1}^{\bullet-}$ salts have been examined.[28,29] Molecular diads having **1** and TTF linked with covalent bridges are being studied for applications in the field of molecular electronics.[30] We chose $\mathbf{1}^{\bullet-}$ for a resonance Raman study because it has the best resolved optical spectrum of the 10 *p*-phenylene-bridged Class III MV compounds studied.[31] Prior Raman studies of $\mathbf{1}^{\bullet-}$ have been published,[32–34] but it was not discussed previously as a MV compound.

NUMERICAL METHODS

Calculation of the absorption spectrum

The fundamental equation for the calculation of the absorption spectrum in the time-dependent theory of spectroscopy is[35]

$$I(\omega) = C\omega \int_{-\infty}^{+\infty} \exp(i\omega t)\left\{ < \Phi|\Phi(t) > \exp(-\Gamma^2 t^2 + \frac{iE_0}{h}t)\right\} dt \quad (1)$$

with $I(\omega)$ as the absorption intensity at frequency ω, E_0 the energy of the electronic transition at the origin, and Γ is a phenomenological damping factor that accounts for relaxation into other vibrational modes of the molecule and to the 'bath'.[36–38] The autocorrelation function keeps track of how the wavepacket Φ develops in time on the excited state potential surface; this surface is treated as being uncoupled from other excited states.[39–43] The total autocorrelation function in a system with *K* orthogonal coordinates is given as

$$< \Phi|\Phi(t) > = \prod_{k=1}^{K} < \varphi^k|\varphi^k(t) > \quad (2)$$

where φ^k is the wavepacket associated with the one-dimensional vector *k* ($k = 1,2,\ldots,K$). The wavepacket φ^k is prepared on the excited state surface by a vertical transition of the lowest energy eigenfunction of the ground state associated with the vector *k*.

Calculation of the resonance Raman enhancement profile

The Raman scattering cross section is given by[36–48]

$$\alpha_{\mathrm{fi}} = \frac{i}{\hbar}\int_0^{\infty} < \varphi_f|\varphi(t) > \exp[i(\omega_i + \omega_l)t - \Gamma t]dt \quad (3)$$

where φ_f is the final vibrational state on the excited state associated with the vertical transition of the particular ground state eigenfunction, $\varphi(t)$ is the time-dependent wavepacket propagated on the excited state surface by the time-dependent Hamiltonian where the $t = 0$ wavepacket is defined by the vertical transition of the lowest energy eigenfunction of the ground state surface, Γ is a phenomenological damping function and $\hbar\omega_i$ is the zero point energy of the ground state surface, and $\hbar\omega_l$ is the energy of the incident photon. The resonance Raman enhancement profile for a particular mode *f* is given as

$$I_{i\to f} \propto \omega_l \omega_S^3 [\alpha_{fi}]^2 \quad (4)$$

where $\hbar\omega_S$ is the frequency of the scattered photon.

RESULTS

We prepared $K^+\mathbf{1}^{\bullet-}$ by the published method.[49] Its absorption spectrum in glassy butyronitrile at 77 K is shown in Fig. 2. The band at 11 751 cm^{-1} is the A_1 band, and that at 22 990 cm^{-1} is dominated by the B_2 band; the B_1 band is calculated to be quite weak and is not resolved.[31] Both bands show vibrational fine structure.

The most enhanced resonance Raman modes of the lowest energy band of $K^+\mathbf{1}^{\bullet-}$ in a KNO_3 salt pellet are reported in Table 1. The absorption spectrum in a KBr salt pellet, a similar environment as KNO_3, shows no vibrational fine structure and shows a maximum absorbance at 16 500 cm^{-1}, close to where the greatest Raman enhancement is observed. Modes at 727 and 980 cm^{-1} are more weakly resonantly enhanced in the Raman profiles, but their distortions were not reliably obtained. The distortions (Δ) are calculated by simultaneously fitting the absorption and the Raman enhancement profiles shown in Fig. 3 using Eqns (1)–(4), which are derived from the time-dependent

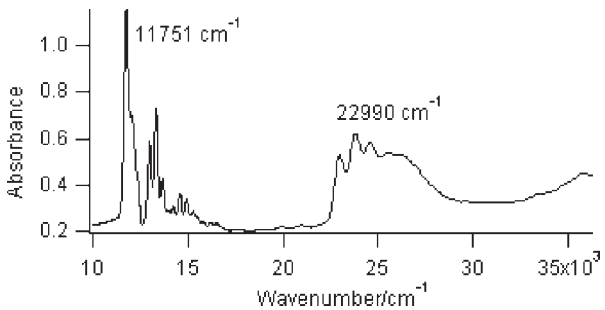

Figure 2. Absorption spectrum of $K^+\mathbf{1}^{\bullet-}$ in butyronitrile at 77 K

Table 1. Resonantly enhanced Raman modes ($\omega_{g.s.}$) of $K^+\mathbf{1}^{\bullet-}$, in a solid KNO_3 pellet, in the lowest energy A_1 transition

$\omega_{g.s.}$	$\omega_{e.s.}$	Δ	λ	Assignment
342	315	0.35	21	Molecular breathing
612	590	0.16	8	*p*-Phenylene breathing
1203	1150	0.16	15	C–N stretch
1393	1250	0.27	51	C=C quinonoid stretch
1608	1590	0.26	54	C=C ring stretch
2215	2000	0.01	0.1	C=N stretch

The excited state frequency ($\omega_{e.s.}$) is determined from the absorption spectrum. The ground and excited state frequencies are used to calculate the distortions. The frequencies and reorganization energy are reported in cm^{-1}.

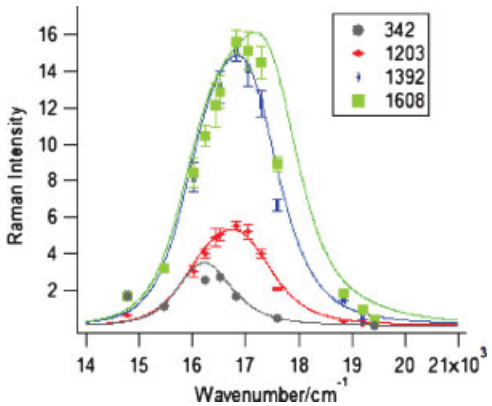

Figure 3. Resonance Raman enhancement profiles and calculated fits of the A_1 transition for the four most enhanced modes of $K^+\mathbf{1}^{\bullet-}$ in a KNO_3 pellet $\Gamma = 900\,cm^{-1}$. The other modes give similar plots

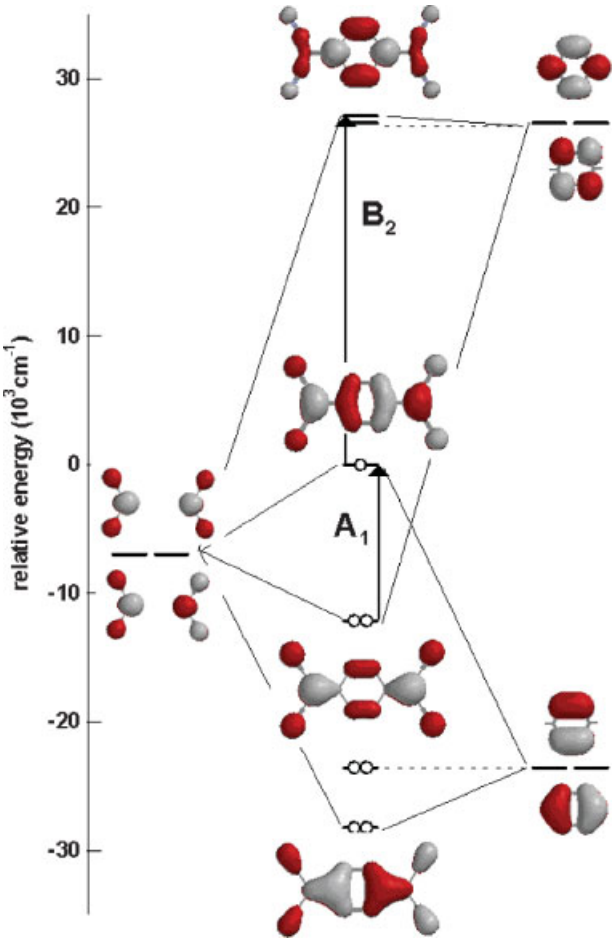

Figure 4. Neighboring orbital diagram for $\mathbf{1}^{\bullet-}$. Benzene MOs positioned at the energy of their non-interacting e component in $\mathbf{1}^{\bullet-}$ are used to represent the diabatic orbitals of the *p*-phenylene bridge, and $^{\bullet}C(CN)_2$ HOMOs are used to represent the diabatic orbitals of the charge-bearing units, which are placed at an arbitrary energy. The intervalence transition is labeled as A_1 (HOMO to SOMO). The excited state mixed valence transition has a dipole allowed and dipole forbidden transition corresponding to the B_2 (SOMO to LUMO + 2) and HOMO to LUMO + 2 transitions, respectively

theory of spectroscopy. The distortions can be interpreted as mode specific reorganization energies ($\lambda = \frac{1}{2}\Delta^2\omega_{g.s.}$). The most distorted mode at $342\,cm^{-1}$ corresponds to a molecular stretching mode along the **M**, **M** axis, the same axis as the polarization of light allowing the electronic transition. The two modes with the highest reorganization energy at 1608 and $1392\,cm^{-1}$ are assigned as the aryl ring stretching and quinonoid stretching frequencies, as in previous work.[33,49]

DISCUSSION

A neighboring orbital diagram[16] that shows the relative energies of the adiabatic orbitals for $\mathbf{1}^{\bullet-}$ calculated using the Koopmans-based method[21,31,50] for the (U)B3LYP/6-31G* calculation at D_{2h} symmetry is shown in Fig. 4. Filled, singly occupied, and unfilled MO energies calculated for open-shell species like MV compounds cannot be directly compared because the orbital occupancies are different, which changes their energies relative to each other by several electron volts.[50] However, the filled orbital MO energy differences for a dianion calculated at the geometry of the radical anion $\mathbf{1}^{\bullet-}$ are close to the transition energies for the Type A transitions (the allowed A_1 band is calculated at $12\,150\,cm^{-1}$, only $400\,cm^{-1}$ too high) and the virtual orbital energy differences for the neutral calculated at the geometry of the radical anion are close to the energies for the Type B transitions (the allowed B_2 band is calculated at $27\,090\,cm^{-1}$, $\sim 4\,100\,cm^{-1}$ high). Type A_{n+1} transitions refer to transitions from *HOMO* − *n* to *SOMO,* type B_{n+1} transition refer to transitions from the *SOMO* to *LUMO* + *n*. Errors become larger as transition energies increase, and other types of transitions than Type A and B become more important.[50] We know of no way other than the Koopmans-based method to obtain reasonable estimates of the energy gaps between MOs with different numbers of electrons in them, which are necessary to draw Fig. 4 and to implement the neighboring orbital method. TD-DFT calculations are designed to give transition energies, and include the effects of configuration interaction on the transition energies.[51–53] Even so, they are significantly further from the experimental transition energies (which obviously include configuration interaction effects), being $2\,470\,cm^{-1}$ high for

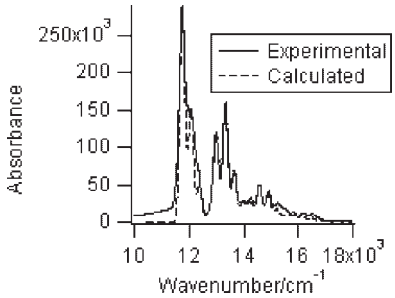

Figure 5. Experimental absorption profile for the lowest energy band $\mathbf{1}^{\bullet-}$ in butyronitrile at 77 K and calculated fit using the data of Table 1 with $\Gamma = 66\,cm^{-1}$

the A_1 band and $3\,980\,cm^{-1}$ for the B_2 band of $\mathbf{1}^{\bullet-}$ than the Koopmans-based method, which does not. Far more expensive CAS-SCF calculations are considerably better for the transition energies but include configuration interaction effects, so they are not the relative adiabatic orbital energy differences desired for a neighboring orbital diagram.[33]

The A_1 transition is assigned as the intervalence or ground state MV transition; in the diabatic picture this corresponds to moving the odd electron from one of the **M** groups to the other. The B_2 transition is the dipole allowed transition in the excited state MV system; the *HOMO* to *LUMO* + 2 transition is the dipole forbidden transition in the excited stated MV system and cannot be unambiguously assigned in the experimental absorption spectrum. In the diabatic picture both of these transitions correspond to moving the odd electron from one of the **M** groups to the bridging group. The energy difference between the dipole allowed and forbidden components of the ESMV system is equal to the energy of the intervalence transition in the model.

We note that the highest reorganization energy bands in Table 1 correspond to the 1608 and $1392\,cm^{-1}$ modes, which is consistent with a formal bond order changes from 2 to 1 between the symmetric *HOMO* and the anti-symmetric *SOMO* that are involved in the transition studied (Fig. 4). The experimental and calculated absorption spectra are compared in Fig. 5. The calculated absorption spectrum gives the excited state frequencies while the ground state frequencies are determined by Raman spectroscopy, both of which as well as the distortions are assumed to be identical for the two solvents used in collecting the spectra.[32] The value of the damping function however must still be different as the spectra are collected at vastly different temperatures. The energy of the electronic transition at the origin is also different for the two solvents being $11\,751\,cm^{-1}$ in butyronitrile and $16\,000\,cm^{-1}$ in KNO_3.

CONCLUSIONS

The optical spectrum of $\mathbf{1}^{\bullet-}$ is most easily understood using the neighboring orbital diagram of Fig. 4. Although $\mathbf{1}^{\bullet-}$ is a Class III MV compound, its lowest energy band maximum should not be interpreted as $2V_{ab}$. The observed transition must be described by a minimum of four interacting diabatic surfaces at three different energies and two electronic coupling; as indicated by the neighboring orbital model. The vibrational fine structure of the first band is rather well calculated using resonance Raman data.

Acknowledgements

We thank the National Science Foundation for support of this work under CHE-0809384 (JIZ), and CHE-0204197 and CHE-0647719 (SFN).

REFERENCES

[1] M. B. >Robin, P. Day, *Adv. Inorg. Radiochem.* **1967**, *10*, 247–422.
[2] G. C. Allen, N. S. Hush, *Prog. Inorg. Chem.* **1967**, *8*, 357–390.
[3] N. S. Hush, *Prog. Inorg. Chem.* **1967**, *8*, 391–444.
[4] R. A. Marcus, *J. Chem. Phys.* **1956**, *24*, 966–978.
[5] R. A. Marcus, N. Sutin, *Biochim. Biophys. Acta* **1985**, *811*, 265–322.
[6] S. F. Nelsen, R. F. Ismagilov, D. R. Powell, *J. Am. Chem. Soc.* **1996**, *118*, 6313–6314.
[7] S. F. Nelsen, *Adv. Phys. Org. Chem.* **2006**, *41*, 183–215.
[8] C. Creutz, *Prog. Inorg. Chem.* **1983**, *30*, 1–73.
[9] A. Broo, S. Larsson, *Chem. Phys.* **1990**, *148*, 103–115.
[10] C. Joachim, J. P. Launay, S. Woitellier, *Chem. Phys.* **1990**, *147*, 131–141.
[11] M. N. Paddon-Row, S. S. Wong, *Chem. Phys. Lett.* **1990**, *167*, 432–438.
[12] M. A. Ratner, *J. Phys. Chem.* **1990**, *94*, 4877–4883.
[13] R. J. Cave, M. D. Newton, *Chem. Phys. Lett.* **1996**, *249*, 15–19.
[14] R. J. Cave, M. D. Newton, *J. Chem. Phys.* **1997**, *106*, 9213–9236.
[15] S. F. Nelsen, Y. Luo, M. N. Weaver, J. V. Lockard, J. I. Zink, *J. Org. Chem.* **2006**, *71*, 4286–4295.
[16] S. F. Nelsen, M. N. Weaver, Y. Luo, J. V. Lockard, J. I. Zink, *Chem. Phys.* **2006**, *324*, 195–201.
[17] J. V. Lockard, J. I. Zink, D. A. Trieber II, A. E. Konradsson, M. N. Weaver, S. F. Nelsen, *J. Phys. Chem. A* **2005**, *109*, 1205–1215.
[18] J. V. Lockard, G. Valverde, D. Neuhauser, J. I. Zink, Y. Luo, M. N. Weaver, S. F. Nelsen, *J. Phys. Chem. A* **2006**, *110*, 57–66.
[19] G. Valverde-Aguilar, X. Wang, E. Plummer, J. V. Lockard, J. I. Zink, S. F. Nelsen, Y. Luo, M. N. Weaver, *J. Phys. Chem. A* **2008**, *112*, 7332–7341.
[20] J. V. Lockard, J. I. Zink, Y. Luo, M. N. Weaver, A. E. Konradsson, J. T. Fowble, S. F. Nelsen, *J. Am. Chem. Soc.* **2006**, *128*, 16524–16531.
[21] S. F. Nelsen, M. N. Weaver, J. P. Telo, J. I. Zink, *J. Am. Chem. Soc.* **2005**, *127*, 10611–10622.
[22] D. S. Acker, W. R. Hertler, *J. Am. Chem. Soc.* **1962**, *84*, 3370–3374.
[23] L. J. Siemons, P. E. Bierstedt, R. G. Kepler, *J. Chem. Phys.* **1963**, *39*, 3523–3528.
[24] J. M. Williams, J. R. Ferraro, R. J. Thorn, K. D. Carlson, U. Geiser, H. H. Wang, A. M. Kini, M. H. Wangbo, In: *Organic Superconductors. Synthesis, Structure, Properties and Theory*, (Ed.: R. N. Grimes), Prentice Hall, New Jersey, **1992**.
[25] J. Ferraris, D. O. Cowan, V. J. Walatka, J. H. Perlstein, *J. Am. Chem. Soc.* **1973**, *95*, 948–949.
[26] G. A. Candela, L. J. Swartzendruber, J. S. Miller, M. J. Rice, *J. Am. Chem. Soc.* **1979**, *101*, 2755–2756.
[27] J. S. Miller, J. H. Zhang, W. M. Reiff, L. D. Preston, A. H. Reis, E. Gerbert, M. Extine, J. Troup, M. D. Ward, *J. Phys. Chem.* **1987**, *91*, 4344–4360.
[28] G. T. Yee, J. S. Miller, *Magnetism—Molecules to Materials*, Vol. 5 (Eds.: J. S. Miller, M. Drillon), Wiley-VCH, Mannheim, **2004**, 223–260.
[29] V. M. Gama, T. Duarte, *Magnetism—Molecules to Materials*, Vol. 5 (Eds.: J. S. Miller, M. Drillon), Wiley-VCH, Weinheim, **2004**, 1–40.
[30] D. F. Perepichka, M. R. Bryce, C. Pearson, M. C. Petty, E. J. L. McInnes, J. P. Zhao, *Angew. Chem. Int. Ed.* **2003**, *42*, 4636–4639.
[31] S. F. Nelsen, M. N. Weaver, J. P. Telo, L. B. Lucht, S. Barlow, *J. Org. Chem.* **2005**, *70*, 9326–9333.
[32] D. L. Jeanmaire, R. P. Van Duyne, *J. Am. Chem. Soc.* **1976**, *98*, 4029–4033.
[33] M. Makowski, M. T. Pawlikowski, *Chem. Phys. Lett.* **2004**, *388*, 367–373.
[34] C.-K. Chi, E. R. Nixon, *Spectrochim. Acta* **1975**, *31A*, 1739–1747.
[35] E. J. Heller, *Acc. Chem. Res.* **1981**, *14*, 368–375.
[36] A. B. Myers, R. A. Mathies, *Biological Applications of Raman Spectroscopy*, Vol. 2, Wiley-International, New York, **1987**, 1–58.
[37] A. B. Myers, *Laser Techniques in Chemistry*, Vol. 23, Wiley, New York, **1995**, 325–384.
[38] A. B. Myers, *Acc. Chem. Res.* **1997**, *30*, 519–527.
[39] C. Reber, J. I. Zink, *J. Chem. Phys.* **1992**, *96*, 2681–2690.
[40] C. Reber, J. I. Zink, *J. Phys. Chem.* **1992**, *96*, 571–576.
[41] J. I. Zink, *Inorg. Chem.* **1973**, *12*, 1957–1959.
[42] M. Henary, J. I. Zink, *J. Am. Chem. Soc.* **1989**, *111*, 7407–7411.

[43] D. S. Talaga, J. I. Zink, *J. Phys. Chem.* **1996**, *100*, 8712–8721.
[44] S.-Y. Lee, E. J. Heller, *J. Chem. Phys.* **1979**, *71*, 4777–4788.
[45] E. J. Heller, R. L. Sundberg, D. Tannor, *J. Phys. Chem.* **1982**, *86*, 1822–1833.
[46] K. S. K. Shin, J. I. Zink, *Inorg. Chem.* **1989**, *28*, 4358–4366.
[47] S. K. Shin, J. I. Zink, *J. Am. Chem. Soc.* **1990**, *112*, 7148–7175.
[48] J. I. Zink, K. S. K. Shin, *Advances In Photochemistry*, Vol. 16, Wiley, New York, **1991**, 119–214.
[49] L. R. Melby, R. J. Harder, W. R. Hertler, W. Mahler, R. E. Benson, W. E. Mochel, *J. Am. Chem. Soc.* **1962**, *84*, 3374–3387.
[50] S. F. Nelsen, M. N. Weaver, T. Bally, D. Yamazaki, K. Komatsu, R. Rathore, *J. Phys. Chem. A* **2007**, *111*, 1667–1676.
[51] K. Burke, E. K. U. Gross, In *Density Functionals: Theory and Applications*, (Ed.: D. Joubert), Springer, Berlin, **1998**, 116–146.
[52] M. E. Casida, C. Jamorski, K. C. Casida, D. R. Salhub, *J. Chem. Phys.* **1998**, *108*, 4439–4449.
[53] R. E. Stratmann, G. E. Scuseria, M. J. Frisch, *J. Phys. Chem.* **1998**, *109*, 8218–8224.